VTT Technical Research Centre of Finland

Sustainable roll-to-roll manufactured multi-layer smart label

Hakola, Liisa; Jansson, Elina; Futsch, Romain; Happonen, Tuomas; Thenot, Victor; Depres, Gael; Rougier, Aline; Smolander, Maria

Published in:
The International Journal of Advanced Manufacturing Technology

DOI:
10.1007/s00170-021-07640-z

Published: 01/12/2021

Document Version
Publisher's final version

The International Journal of Advanced Manufacturing Technology (2021) 117:2921–2934
https://doi.org/10.1007/s00170-021-07640-z

ORIGINAL ARTICLE

Sustainable roll-to-roll manufactured multi-layer smart label

Liisa Hakola[1] · Elina Jansson[1] · Romain Futsch[2,4] · Tuomas Happonen[1] · Victor Thenot[3] · Gael Depres[3] · Aline Rougier[2] · Maria Smolander[1]

Received: 10 May 2021 / Accepted: 5 July 2021 / Published online: 19 August 2021

Abstract
Sustainability in electronics has a growing importance due to, e.g. increasing electronic waste, and global and European sustainability goals. Printing technologies and use of paper as a substrate enable manufacturing of sustainable electronic devices for emerging applications, such as the multi-layer anti-counterfeit label presented in this paper. This device consisted of electrochromic display (ECD) element, NFC (near field communication) tag and circuitry, all fully roll-to-roll (R2R) printed and assembled on plastic-free paper substrate, thus leading to a sustainable and recyclable device. Our setup uses harvested energy from HF field of a smartphone or reader, to switch an electrochromic display after rectification to prove authenticity of a product. Our novelty is in upscaling the manufacturing process to be fully printable and R2R processable in high-throughput conditions simulating industrial environment, i.e. in pilot scale. The printing workflow consisted of 11 R2R printed layers, all done in sufficient quality and registration. The printed antennas showed sheet resistance values of 32.9±1.9 mΩ/sq. The final yield was almost 1500 fully printed devices, and in R2R assembly over 1400 labels were integrated with 96.5% yield. All the assembled tags were readable with mobile phone NFC reader. The optical contrast (ΔE*) measured for the ECDs was over 15 for all the printed displays, a progressive switching time with a colour change visible in less than 5 s. The smart tag is ITO-free, plastic-free, fully printed in R2R and has a good stability over 50 cycles and reversible colour change from light to dark blue.

Keywords Printed electronics, · Electrochromic display, · Sustainability, · Anti-counterfeiting

1 Introduction

Definitions for sustainability highlight that humans have to act for the benefit of environment, but at the same time develop solutions that help future generations to survive [1, 2]. Circular economy is closely linked to sustainability, and it expects that more durable products are designed and manufactured, renewable materials are used in their manufacturing without generating extensive manufacturing waste, and products are reused, recycled or repaired efficiently [3].

Motivation for electronics industry to utilize these principles and decrease environmental impact comes from global and European sustainability actions, such as European Green Deal and United Nation's Sustainable Development Goals, but also from particular industrial trends. The global electronic waste is the fastest-growing domestic waste stream projected to double between 2014 and 2030 [4, 5] with only 20% of this recycled properly [6, 7]. This means that valuable components and materials end up in environment, and many of these can be toxic. At the same time, the global consumption of materials is expected to more than double during the next decades [8] concerning also rare and valuable materials used for electronics. Furthermore, new types of electronic solutions are emerging that at some point of their lifecycle end up in biological environment, either in purpose or accidentally. Examples include sensors for intelligent packaging, environmental monitoring, disposable diagnostics and precision agriculture.

✉ Liisa Hakola
liisa.hakola@vtt.fi

[1] VTT Technical Research Centre of Finland Ltd., Espoo, Oulu, Finland

[2] CNRS, Univ. Bordeaux, Bordeaux INP, ICMCB (UMR 5026), F33600 Pessac, France

[3] ArjoWiggins France, 38500 Voiron, France

[4] Luquet&Duranton, 07100 Annonay, France

For electronics industry, sustainability can be considered through different aspects, also as a combination of multiple aspects [9–12]. New materials originating from renewable resources can replace some of the current materials, such as fossil-based polymer and composite substrates. Many of these materials can be compostable or bio-degradable making them ideal for solutions where material recycling is not the most feasible option. Another aspect is utilization of energy and material efficient manufacturing processes, such as additive printing methods. It is estimated that additive manufacturing processes powered by electricity generated from renewable energy, uses one tenth of the materials of traditional factory production, resulting in a clear reduction in CO_2 emissions and the use of the earth's resources [13]. At the same time the material consumption decreases [14]. Recycling, reuse and repair models of components and materials can help to recover material value currently lost for landfill and incineration in electronic waste. Eco-design and circular design approaches aim to design electronic components and devices in a way that minimizes material and energy consumption throughout the life-cycle and value chain, and eases up disintegration during recycling. Examples include minimal material use and waste generation, or use of renewable materials.

This paper takes a sustainable approach for electronics by using paper as a substrate material and high-speed roll-to-roll (R2R) printing as the main manufacturing method in order to demonstrate an electronic anti-counterfeit label. This label consists of an electrochromic display (ECD) element and Near Field Communication (NFC) tag designed for guaranteeing authenticity of a product. When in contact with an NFC reader, the display element changes colour to indicate a genuine product. The novelty in our paper is to combine an NFC tag and electrochromic display on a paper substrate by using only high throughput R2R printing and assembling technologies.

Electrochromic devices consist of two electrochromic (EC) layers separated by an electrolytic layer [15]. EC materials have the capability to change their optical properties through chemical oxidation or reduction when submitted to an applied voltage. ECDs can operate in either reflecting or transmitting mode. They are considered low cost display devices, and to consume little power, since the change from one state to another requires minimal energy in a matter of seconds. For printed ECDs conductive polymers are typically used as the electrochromic material [16–20]. The electrolyte is often an ultra violet (UV) curable polymer material. Electrodes are usually indium tin oxide (ITO) that is a transparent conductor or metal based inks. Polymers, such as PET (polyethylene terephthalate) or PEN (polyethylene naphthalate) are typical substrates, but other substrates have also been evaluated, such as textiles by Wei et al [21]. Pietsch et al have demonstrated a bio-degradable EC display for sustainable short-life cycle electronics [22]. This display comprised of a poly(3,4-ethylenedioxythiophene): polystyrene sulfonate (PEDOT:PSS) electrochromic layer, a gelatin-based electrolyte and gold electrodes deposited on a cellulose di-acetate substrate. The printed devices showed an electrochromic contrast of 32 ± 4% and switching times of 3.0 ± 1.4 s, comparable to the spin coated reference devices.

Herein, the printed electrochromic display is fabricated using a vertical architecture, meaning that each layer is printed and cured on top of another layer as shown in Fig. 1. In general, vertical architecture shows a faster switching from one colour to another compared to coplanar architecture for a similar surface, where the two electrodes are printed side-by-side [23]. Indeed, the space between the two electrodes is limited by the printing resolution obtained with screen-printing and that is the main reason why vertical architecture was chosen. The two electrodes are necessary for applying an electrical potential difference, and the electrolyte to move the charges which are responsible for the redox reaction in electrochromic material. This redox reaction is responsible of the colour change of the electrochromic material. All the layers are printed on a single paper substrate and is encapsulated both at the level of the substrate and on top of the ECD for protecting the device from its environment.

Paper-based electronics is a widely studied area. Paper has been evaluated as a substrate for thermochromic and electrochromic displays, resistive memory devices, transistors, disposable radio frequency identification (RFID) tags, batteries, photovoltaic cells, and sensors and actuators [24–27] . Using paper as a substrate for printed electronics has obvious advantages such as low cost, flexibility, biodegradability, compostability and ease of disposal through fibre recycling or incineration. Paper's many applications make it an attractive substrate, but its high roughness, absorbency, poor barrier properties and sensitivity to elevated moisture levels are often considered to create challenges for printed electronics [28]. Intelligent packages are often mentioned as one of the most promising area for paper based electronics [29], and the anti-counterfeit label described in this paper targets that domain. The goal of intelligent packaging technologies is to provide means for controlling packed product quality, to provide more convenience to consumers, to market and brand the products, and to control counterfeiting and theft [30].

There are examples in literature of similar type of printed components as described in this paper, even on paper substrate. Wang et al have demonstrated inkjet-printed RFID antennas on paper substrate by using surface modification and electroless deposition (ELD) to gain low enough resistance [31]. Islam et al have also used inkjet-printed silver nanoparticle ink on paper to manufacture RFID antennas for sensor applications [32]. Here the antenna consisted of modified meander line radiator with a semi-circular shaped feed network. Nunes et al have demonstrated electrochromic paper based

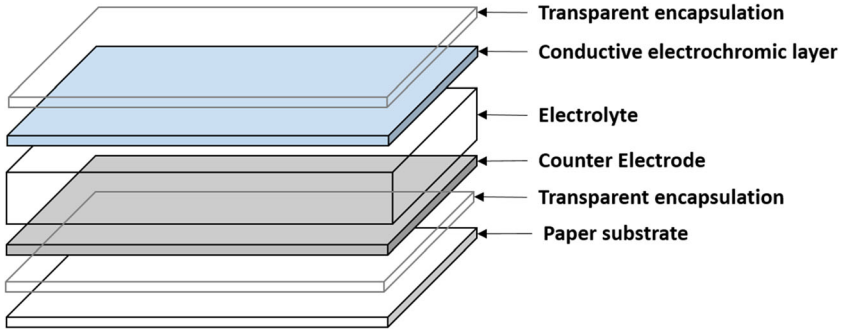

Fig. 1 Paper-based electrochromic display structure with a vertical architecture

displays by using TiO_2 (titanium dioxide) nanostructured films [33]. However, the deposition is based on a microwave-assisted hydrothermal method at low temperature, not on printing. Lang et al. have shown that inkjet-printed PEDOT:PSS-based electrodes can be used for electrochromic displays, but besides the electrodes the other parts of the display have not been printed [34]. In these earlier works, only parts of a component have been manufactured by printing contrary to our work where all parts of an electronic device are printed or R2R processes. There are some examples of fully printed structures also. Andersson Ersman et al. have manufactured fully screen printed electrochemical transistors based on, e.g. PEDOT:PSS, printable electrolyte and carbon ink, but they have used PET (PolyEthylene Terephtalate) as a substrate [35].

Printed electronics is often said to enable 'electronics everywhere' [36]. This causes a challenge to be able to collect and manage these devices from different waste streams, for example, the paper-based anti-counterfeit labels described in this paper. Our paper also discusses the impacts of paper based electronics from the material recyclability point of view. According to Furuta et al. [37] and Erdmann et al. [38], electronic components can influence the composition of solid and liquid residues in paper recycling process, and thereby affect disposal costs. The increasing amount of adhesives in the pulp coming from component assembly and electronic label attachment may result in an increase of agglomerated adhesives and fibres, already a recognized issue resulting also from other sources of adhesives.

Aliaga et al. have evaluated how electronic components affect paper recycling [39]. Their observation was that presence of printed electronic components did not increase the fibre rejects during paper recycling, and properties of the recycled paper were not significantly affected by the presence of components. In their study the assembled components were blocked in the sieving systems. However, in the future, it is likely that more and more electronic components will be attached to paper based products, such as packages, and more efficient collection and recycling of these components will be required. In addition, design and manufacturing of smart packaging solutions, such as the anti-counterfeit label presented in this paper, can advance also treatment and recycling of packaging waste [40]. One opportunity is utilization of biodegradable materials, such as the paper substrate used here. Furthermore, one challenge is electronic material identification and separation from other waste. Chen et al. proposed recording and tracing the lifecycle information, thus optimising disassembly process and improving recovery efficiency [41].

2 Materials and methods

2.1 Device structure and operation principle

Figure 2 shows the smart label in the case where the NFC chip is read with the smartphone and thus enabling the ECD to change colour. The final printed design of the ECD has a size of a credit card (86*54 mm^2) where the electrochromic surface, i.e. surface where the colour change operates, has a surface of 0.95 mm^2. Characteristics of the antenna were evaluated thanks to a simulation before the printing. Measurements are in line with the simulated values with an increased value of the capacitance. Finally, the chip selected for the activation was the AS39513 (ams AG, Austria) which delivers a sufficient high voltage for the electrochromic display change of colour.

2.2 Printing

The ECD element, antenna, and wirings were rotary screen printed onto a 95-μm-thick paper substrate PowerCoat HD from Arjowiggins Creative Papers using an R2R printing line at VTT. This printing line consists of a single interchangeable printing unit followed by four hot-air box ovens and two moveable UV-curing units. The maximum printing speed of the line is 10 m/min and the length of the web path between the un-winder and re-winder is 20 m. The total length of the box ovens is approximately 3.6 m and the maximum temperature of the ovens is 140°C. Due to the limited oven length, the printed layers are often re-run through the printing line to perform an extra drying cycle, thus ensuring complete drying

a)

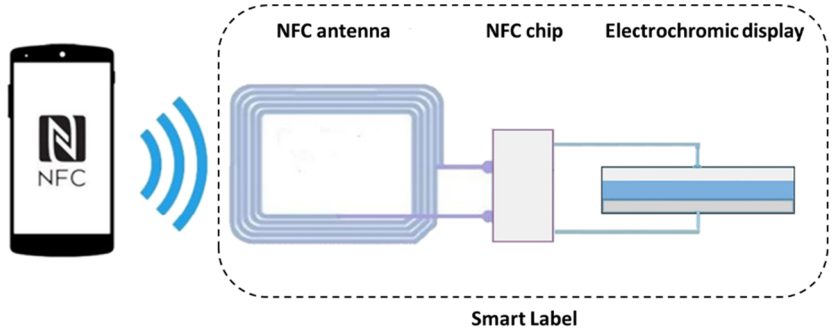

b)

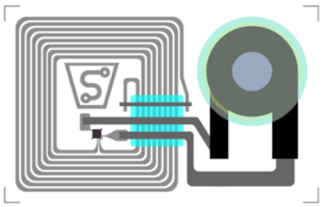

c)

Dimension	48 x 46 mm	
Number of turns	8	
Line width	0.9 mm	
Line gap	0.6 mm	
Total length	≈ 114 cm	
Ink surface	≈ 10.2 cm²	
	Simulation	**Measurement**
Electrical resistance [Ω]	30.9	**28.5**
Inductance [µH]	3.15	**3.18**
Capacitance [pF]	8.5	**10.8**
Resonant frequency [MHz]	13.6	**13.2**
Quality factor	8.7	**9.5**

d)

AMS AS39513	
NFC Standard	ISO15693 + NFC Forum type 5
Dimensions (mm)	2.31 x 2.4 x 0.3
EEPROM Memory	9Kbit
ADC input	1 input for resistive or voltage based sensors
Supply Voltage	1.5 or 3V battery (single or dual-cell)
Internal sensor	Temperature / -20 to 55°C
Other Features	Energy harvesting output (3mA) from RF field Bus SPI slave Real-Time-Clock (RTC) Logging capacity up to 1020 events Low energy consumption (≈1 year with 30 mAh battery) Logging event can be triggered by external sensor
Cost	Less than 1€ (Quantity > 50.000)

Fig. 2 (a) Schematic of the smart label structure activated using the NFC function of a smartphone. The device is made of a fully-printed electrochromic display and NFC antenna. The NFC chip is transferred on the device using a pick-and-place equipment. (b) Final design of the smart label (c) NFC antenna main properties with performance simulated and measured. (d) Main feature of the NFC chip selected for the display colour change

and optimized conductivity of the printed layers. In this paper, totally eleven layers were printed, dried or cured, and registered on the top of each other. All the layers were printed in separate print runs. Figure 3 shows the printed layer stack, the printing layout, the rotary screen printing process, and the final printed multi-layer device prior to the R2R assembly. In total, over 2000 devices were manufactured which corresponds to the total run length of 80 m.

The paper substrate was thermally pre-treated twice in the R2R printing line prior to the printings at 140°C using the process speeds of 2 m/min and 4 m/min. The total dwell time in the drying ovens was approximately 2.7 min. This pre-treatment ensured a better dimensional stability of the substrate during the multilayer printing and drying/curing processes, thus enabling more accurate layer-to-layer alignment and optimized device performance.

Both silver layers, Layer1 and Layer5, were rotary screen printed with Asahi LS-411AW silver paste using a stainless steel Rotaplate® screen with a mesh count of 215 lines/inch from SPGPrints. The printing speed was 2 m/min and the

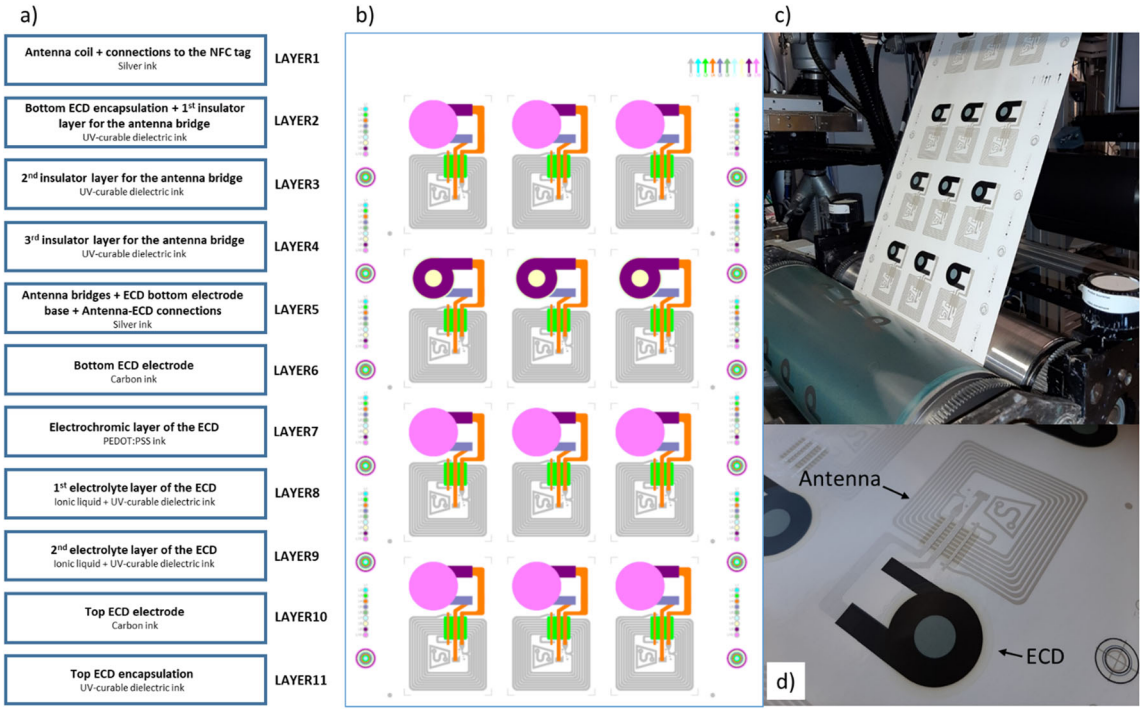

Fig. 3 The layer stack of the R2R printed device (a), the printing layout (b), and the rotary screen printing of the top ECD electrode layer (c), and the final device prior to the assembly of the NFC tag (d). The printing layout, i.e. a single repetition length, contains 12 individual devices of which three of them are manufactured without any encapsulation layers. The length of the single repetition is approximately 41 cm

drying temperature of the ovens was set to 140°C. An extra drying cycle at the speed of 3 m/min was performed at 140°C to optimize the layer conductivity. The total dwell time in the drying cycles was approximately 3 min.

UV-curable DuPont 5018A dielectric paste was used to print all the three insulator layers for the antenna bridges (Layer2-4) as well as top and bottom ECD encapsulation layers (Layer2 and Layer11). The first bridge insulator layer was printed simultaneously with the bottom encapsulation layer, thus establishing Layer2. The printing speed of all the layers printed with DuPont 5018A was 4 m/min. These printed dielectric layers were separately cured directly after their deposition using a single on-line UV-curing unit at the power level of 50 %. The peak wavelength of the UV lamp of the curing unit is 365 nm and its maximum power level is 160 W/cm. The estimated curing time of each layer printed with DuPont 5018A was 2.3 s. The same screen type was used with Layer2, Layer3, and Layer11 as in the case of the silver layers but Layer4 was printed using a coarser SPGPrints' Rotaplate® screen with a mesh count of 125 lines/inch.

The top and bottom electrode layers, i.e. Layer6 and Layer10, were printed with Loctite EDAG PF 407A E&C carbon paste at a speed of 3 m/min. The drying temperature was set to 140°C and the drying cycle was performed twice, thus making the total drying time approximately 2.4 min. The carbon layers were printed using SPGPrints' Rotaplate® screens. The mesh count of the bottom carbon electrode layer (Layer6) was 305 lines/inch whereas a mesh count of 215 lines/inch was used in the case of the top carbon electrode layer (Layer10) to ensure better coverage of the underlying thick printed layer interfaces.

The electrochromic layer (Layer7) was rotary screen printed with AGFA ORGACON EL-P5015 PEDOT:PSS paste. The printing speed was 2 m/min, the drying temperature was set to 140°C, and the drying time was approximately 1.8 min. No extra drying cycle was used with this layer. The mesh count of the screen was 215 lines/inch (SPGPrints Rotaplate®).

Two electrolyte layers (Layer8 and Layer9) were printed using a self-formulated paste: 40 wt-% of ionic liquid (LiTFSI-EmimTFSI, 1:9 mol.% from Solvionic) was mixed with 60 wt-% of UV-curable dielectric paste (5018A from DuPont). Both electrolyte layers were printed at the speed of 4 m/min and cured using two separate UV curing units of the printing line at power levels of 50 % (Curing unit 1) and 22 % (Curing unit 2). The use of the two UV curing units in the case of the both electrolyte layers increased the curing time, thus making the electrolyte layers less sticky in the R2R process. The lower power level of the 2nd curing unit was selected to avoid yellowing of the electrolyte layers during the prolonged curing. Both electrolyte layers were printed using the same screen type but two different screen types were used to manufacture ECDs with different electrolyte layer thicknesses.

The mesh counts of the screens were 215 lines/inch (SPGPrints) and 88 lines/inch (Gallus Ferd. Rüesch AG).

2.3 Component assembly

Followed by R2R printing, NFC chips were bonded on smart labels by maintaining the roll format. The R2R assembly line includes two dispenser robots, automated pick-and-place machine as well as heat-treatment and UV-curing units. The 18-meter long line is capable of performing all these processing steps in a stop-and-go mode during the same run. In this study, a working area to be processed at once included 12 labels printed on a 409,575 mm * 270 mm area as depicted in Fig. 3.

The first processing step was applying isotropic conductive adhesive (ICA) dots on each chip interconnection areas by the first Dima Elite Dispenser DR-61 dispensing robot. Here, Epotek H20E-PFC was utilized as the conductive adhesive. The glue was dispensed through a jet valve resulting in about 200 μm dots in diameter. Next, assembly of chips on wet adhesive dots was done by Fuji pick-and-place machine. The components were fed for assembly process from a tape carrier after taping and reeling the bare dies from a wafer to a tape. Subsequently, the web went through an oven set at 120°C temperature. Over 15 min time spent in the elevated temperature was accordant to the curing profile preferred by adhesive manufacturer. Next to heat-treatment, the dies were mechanically bonded on the substrate by utilizing a UV-curable non-conductive adhesive (NCA). The second Dima DR-61 dispenser robot was configured to dispense Dymax 9008 adhesive around the chip sides to enhance their mechanical stability. The final step covered curing of NCA under a UV-LED illumination at 365 nm for less than minute. Figure 4 depicts the R2R assembly line and its main process used when manufacturing NFC smart labels.

2.4 Characterisation

The layer thickness of each layer was separately measured with Veeco Dektak 150 surface profilometer. The surface roughness (R_a, R_q) of the printed layers was measured with Veeco Wyko NT3300 white-light interferometer. The measurement area was 297*226 μm^2. The visual quality and spreading of the layers was evaluated and measured with OGP® (Optical Gaging Products) SmartScope 250 microscope. In order to evaluate the performance of the device prior to the assembly, the open circuit voltage of the electrochromic display and the sheet resistance of the antenna were determined with a digital multimeter FLUKE 289.

Smart labels were activated directly with the NFC function of a smartphone (Huawei P smart 2019) without any previous application download. The electrochemical performance of the ECD were characterized using a BioLogic SP50 potentiostat/galvanostat apparatus. Colourimetry analysis was carried out using a Konica Minolta CM-700D spectrophotometer with a SCE 10°/D65 configuration. The colourimetric parameters of the CIE (L*, a*, b*) colour space and the optical contrast between initial and reduced states can directly be determined with itl (Konica Minolta Sensing Europe B.V). The apparatus was connected to a computer with the software SpectraMagic for enabling the measurement of colourimetric parameters every second.

Fig. 4 R2R assembly line overview (a), including jet valve for ICA dispensing (b), pick-and-place machine for chip assembly (c), and needle valve for NCA application (d)

3 Results

Printing of the different layers was carried out as the first step. The electrochromic displays were then characterized and finally the chips were assembled.

3.1 Printing

All the layers can be successfully printed at good quality and with well-defined edges onto the paper substrate as well as on the top of each other using the R2R rotary screen printing process, as shown in Fig. 5. The printed layers have good coverage and they can also cover the interfaces between the paper and the underlying layers without any discontinuities. The printed layers remain nicely on the surface of the paper and do not penetrate excessively into the paper structure, thus improving both the visual quality and performance. In addition, the layers are accurately aligned with each other due to the minimized dimensional changes of the paper during the thermal pre-treatment cycles, thus optimizing the device performance even further. It is also noticed that when the electrolyte layers are printed with the coarser screen (88 mesh/inch), the edge definition decreases due to the larger screen openings but at the same time the layer thickness increases significantly, thus in turn improving the device performance. However, the printing of these thicker electrolyte layers lead to some curing issues as a result of which some ionic liquid from the surface of the printed electrolyte layers sticks onto the process rollers and onto backside of the paper once rewound. The ionic liquid part of the ink tends to remain in liquid form even after the curing. Therefore, the ionic liquid content in the electrolyte ink should be carefully optimized for every ink transfer volume separately.

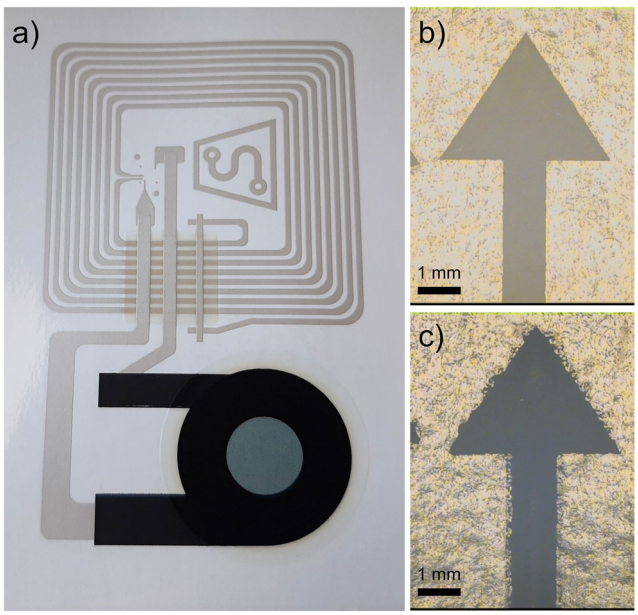

Fig. 5 Print quality of the device stack (a). The use of the finer screen (b) with the electrolyte layer leads to more well-defined edges but thinner layer than with the coarser (c) screen

Table 1 presents the layer properties of each layer of the final device. The PEDOT:PSS layer is the thinnest because of the low solids content (3–5 wt-%) of the ink, and a thicker layer would not give optimal colour change. The thickness of the PEDOT:PSS layer can only be estimated since the layer sinks mainly into the irregularities of the paper with the average roughness (R_a) of 1.2 μm. As expected, the multilayer printing of insulator and electrolyte layers using high solids content UV-curable inks and coarser screens increases the layer thickness to several tens of micrometers. The smoothest layers are achieved with the electrolyte layers since the thick layers can cover and fill the irregularities of the substrate as well as underlying layers. In addition, the ionic liquid component of the electrolyte ink aids in the layer levelling, i.e. smoothening, after the ink transfer onto the substrate by keeping the ink easily flowable prior to the UV-curing. All the printed layers spread less than 50 μm. This small spreading ensures a good device performance by enabling accurate alignment accuracy and keeping the ink layer from spreading onto un-desired areas. The spreading tends to increase with coarser screens. The smallest spreading is seen with the silver and PEDOT:PSS inks.

The printed antennas (Ag1) on the paper have low and even sheet resistance values of 32.9±1.9 mΩ/sq., thus indicating a good and stable readability and functionality of the device. In addition, the Ag2 layer has a sheet resistance of 37.8±6.4 mΩ/sq. which ensures a proper conductivity of the bridges, wirings, and bottom electrode. The electrochromic display part is also functional and all the tested display parts are functional. The open circuit voltage (OCV) of the electrochromic display is 45.6±8.0 mV and 62.9±3.6 mV for the electrolyte layers printed with 215 lines/inch and 88 lines/inch screens, respectively. The increase in the layer thickness not only increases the OCV but also decrease its deviation, thus showing better repeatability. However, at the same time, the proper curing and printability of the electrolyte layer becomes more difficult. After these initial performance tests, the printed devices on the paper surface could be assembled in a R2R process.

3.2 Electrochromic display characterisation

In order to characterise the display colour change, the optical contrast (ΔE*) is used in electrochromism. This data gives a good indication if there is a difference between one state associated to a colour and a second state associated with a different colour once the redox reaction took place. ΔE* is defined thanks to the chromaticity parameters (L*, a*, b*) which belong to the CIE colourimetric space [42]. For PEDOT:PSS, a cathodic coloration material, the colour change switches from the oxidized state (L^*_{ox}, a^*_{ox}, b^*_{ox}) which corresponds

Table 1 Properties of the printed layers. The spreading is measured for a single printed layer (*). The thickness value represents the total layer thickness

Layer		Thickness (μm)	Ra roughness (μm)	Rq roughness (μm)	Spreading of 1000 μm line* (μm)
Antenna + wirings (Ag)	LAYER 1	12.9 ± 1.3	0.9 ± 0.1	1.2 ± 0.1	−1
ECD bottom encapsulation (UV dielectric)	LAYER 2	17.0 ± 1.5	1.2 ± 0.2	1.8 ± 0.4	40
Insulation of the antenna bridges (3 layers – UV dielectric)	LAYER 2–4	65.6 ± 5.0	1.4 ± 0.3	1.7 ± 0.3	46
Antenna bridges, antenna-ECD connector, ECD bottom electrode (Ag)	LAYER 5	14.3 ± 1.9	0.9 ± 0.1	1.2 ± 0.1	−3
ECD bottom electrode (Carbon)	LAYER 6	3.6 ± 0.5	1.2 ± 0.1	1.5 ± 0.1	24
ECD electrochromic layer (PEDOTS:PSS)	LAYER 7	1	0.7 ± 0.1	0.9 ± 0.1	−7
ECD electrolyte layers	LAYER 8–9				
(2 layers – ionic liquid + UV dielectric)	215 mesh/in.	30.3 ± 3.6	0.4 ± 0.04	0.6 ± 0.1	24
	88 mesh/in.	80.5 ± 4.9	0.4 ± 0.02	0.6 ± 0.1	47
ECD top electrode (Carbon)	LAYER 10	5.1 ± 0.6	1.1 ± 0.1	1.4 ± 0.2	40
ECD top encapsulation (UV dielectric)	LAYER 11	17.8 ± 1.9	0.8 ± 0.2	1.0 ± 0.2	32

to the as-deposited colour, to a reduced state (L^*_{red}, a^*_{red}, b^*_{red}) (Equation (1)).

$$\Delta E^* = \sqrt{\left(L^*_{red} - L^*_{ox}\right)^2 + \left(a^*_{red} - a^*_{ox}\right)^2 + \left(b^*_{red} - b^*_{ox}\right)2} \quad (1)$$

The higher optical contrast between two states, the easier it will be for a human eye to distinguish between two colours. It is considered that a ΔE* value higher than 10 is necessary to distinguish two colour states [43].

For this application, the second most important parameter in electrochromism concerns the switching time, which is defined as the time necessary to observe the colour change. In this study, the L*, a*, b* values of displays were measured every second during a chronoamperometry (CA). The CA consists in the measurement of the current density when applying a potential difference between the two electrodes of the ECD for a defined time.

Figure 6 shows the visual and optical performance of the fabricated displays. Four conditions were investigated: either 80 μm thick electrolyte (88 L/inch) or 30 μm thick electrolyte (215 L/inch). Furthermore, the impact of the encapsulation on the performance was also studied. The final encapsulation layer has a positive impact on the optical contrast. For 88 L/inch electrolyte ΔE*increases of 13% whereas it is of 34% for 215 L/inch electrolyte. The PEDOT:PSS layer shows higher L* value and a positive b* value leading to a more colourless layer when there is an encapsulation, but the difference is marginal.

Figure 7 shows the chronoamperograms of the 4 different displays. Small differences are observed when the ECD is top encapsulated especially for the 30 μm thick electrolyte. Without encapsulation, the thickness of the electrolyte does not seem to have an impact on the current density. A small leakage current (from 0.15 to 0.30 mA/cm^2) is measured when E = -3.8V which is probably linked to the interface between the carbon electrode and the electrolyte that needs to be further optimized. The leakage current seems to be reduced when the device is top encapsulated.

Figure 8 a) shows the variation of the optical contrast versus time for a unique $E = -3.8V$ that simulates the operating mode for the smart label. The study was only performed on the 80 μm thick electrolyte leading to a uniform colour change on the full surface on the contrary to the 30 μm thick electrolyte. This measurement shows a progressive change of colour with a faster and more intense optical contrast between the initial (neutral) and the reduced state with an encapsulated device. The colour change starts to be observable 5 seconds after the potential difference is applied corresponding to an

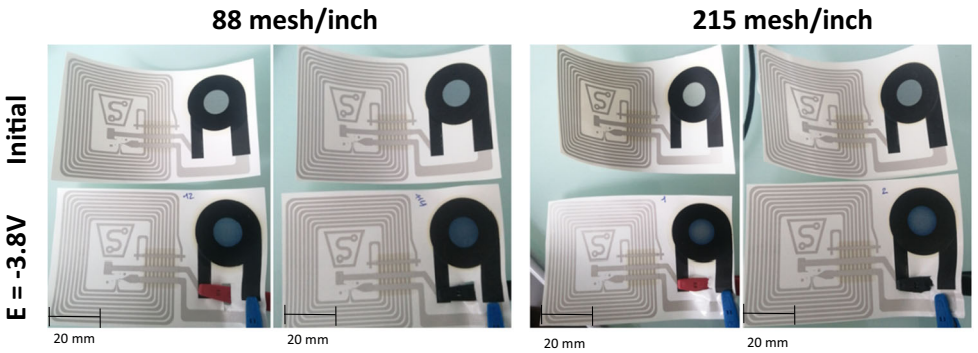

	Encapsulation		No encapsulation		Encapsulation		No encapsulation	
	Initial	-3.8V	Initial	-3.8V	Initial	-3.8V	Initial	-3.8V
L*	57.4	45.8	53.5	43.5	59	39.8	57.3	44
a*	-5.8	-5.6	-4.9	-4.2	-5.3	-4.6	-5.3	-3.5
b*	1.7	-11.2	-1.5	-12.6	5.46	-12.3	-1.8	-12.7
ΔE*	17.3		15		26.2		17.3	

Fig. 6 Visual and colorimetric parameters measurement comparison between the oxidized/neutral and the reduced states, recorded after a CA at E = -3.8V for 30 seconds of the fabricated R2R displays before the chip pick-and-place

optical contrast reaching a value of 10. The maximum of optical contrast is limited by the PEDOT:PSS in this configuration as a slower increase of ΔE* after 10 seconds of applied voltage is observed.

As shown on the Fig. 8 ab), the ECDs do not keep the colour parameters of the reduced states once the potential difference is removed. The switching time for a surface of 0.95 cm^2 from reduced to initial state decreases when the device is top encapsulated. Overall, the ΔE* (in accordance with the initial values) reaches a value lower than 10 in 3 min; ΔE* further decreases to 4 and 6 (without encapsulation) after 15 minutes with and without encapsulation, respectively. On rest, the display will slowly come back to its original colour after some time (1h).

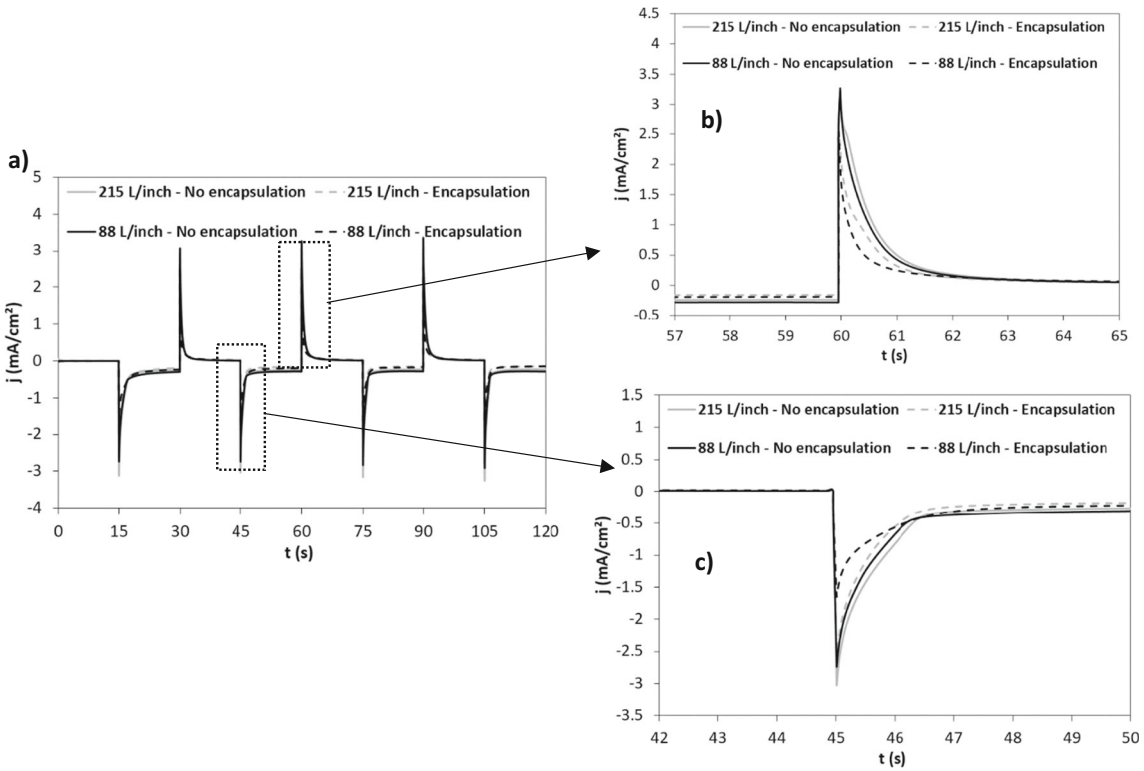

Fig. 7 Chronoamperograms of the displays presented in Fig. 6) CA with E = 0 ; -3.8V for 15 seconds for each potential and 3 cycles. b) Magnification on the oxidized state (E = 0V). c) Magnification on the reduced state (E = -3.8V)

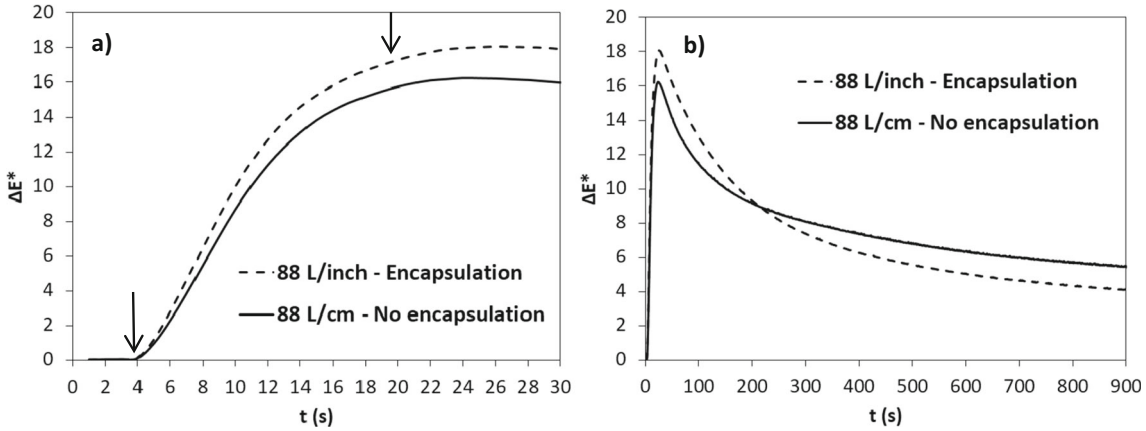

Fig. 8 a) Variation of the optical contrast ΔE* with time when $E = -3.8$V is applied for 15 s (the time interval is marked with the two arrows) and b) variation of the optical contrast ΔE* with time in open-circuit (from t = 20s). Colorimetric parameters were measured every second

Displays were switched more than 50 times using this condition (−3.8 V for 15 s) and no performance degradation was observed for the optical contrast and the switching time.

The results obtained show promising results for a R2R fully-printed ITO- and plastic-free ECD thanks to the use of a new electrochromic display architecture.

The ECD design still needs some optimization in order to reduce the number of steps, improve the switching time from the neutral to reduced state and the optical contrast. The current ECDs have an optical contrast above 15, a progressive colour change visible in less than 5 seconds on the full electrochromic surface and a stability in time, with more than 50 cycles tested in a smart label real application. The display returns to its original state, or a close colour, after 15 min rest. The encapsulation improves the performance of the ECD, it would also be rewarding to test the stability of the device with accelerating degradation factors (temperature, humidity…) to simulate the performance on long term and the efficiency of the encapsulation.

3.3 Component assembly

From chip bonding perspective, the most critical part was ICA dispensing. In particular, there were tight tolerances in terms of dispensing accuracy and spreading of adhesive dots to establish functional interconnections. The dispensing recipe was optimized to form adhesive dots with sufficient volume for electrical and mechanical bonding, but avoiding short circuits between adjacent dots. Figure 9 shows the locations of applied adhesive dots with respect to printed silver layer and how they are spread after assembly and curing. A wet dot is spread from about 200 to 350–400 μm in diameter due to pressure caused by component placing operation, and thus to be taken into considerations when designing a dispensing routine.

The throughput in R2R assembly is defined by the slowest parallel process phase. This is due to stop-and-go type operation mode, where the roll is moved as each active process is finished. In this assembly task, both ICA and NCA dispensing were significantly slower than pick-and-placing. The time spent for dispensing operation in both cases was about 2 min including indexing time for web movement. This corresponds to 10 s for a label in average or 360 labels per hour, or about 5 min per meter as the throughput. Within the 2 min processing time spent in dispensing, a substantial amount of time was taken by fiducial checks. Reducing the number of fiducials per working area would increase the throughput, but also increases the risk for misplaced adhesive dots.

There were 119 working areas assembled in total, from which 42 were printed with 88 lines/inch screens and 77 working area with 215 lines/inch, respectively. This equaled to 1428 assembled labels, or close to 50 meters of assembled foil. After the assembly process, functionality of each smart label was tested via a mobile phone and a generally available NFC application. As a result, 50 out of 1428 chips from all the R2R produced samples were not detected via NFC. This meant 96.5 % yield for the bonding process in terms of chip functionality in wireless communication. Taking in account only the ECD, the 50 displays, where the chip was detected, were switching colour with a potential difference of 3.8V applied thanks to a potentiostat. In other word, the yield loss is only linked to the chip pick-and-place process and is therefore not linked to the display fabrication where the working yield reach 100%.

4 Discussion

Sustainability of the developed device is discussed here both from environmental and economical perspective.

A life cycle assessment (LCA) was carried out to determine exactly how resource-efficient printed electronics on paper are and where potential for improvement is needed. Replacing organic or inorganic substrates with paper in manufacturing simplifies subsequent recycling and reduces waste both during

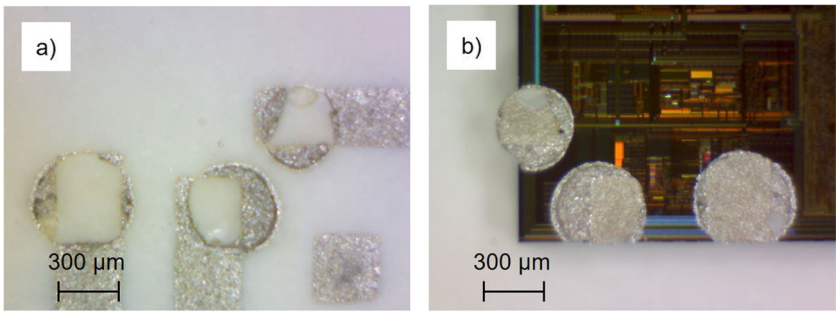

Fig. 9 Adhesive dots after detaching an assembled die on top of the substrate (a) and below a chip (b)

processing and at the end of the product's life. Printing processes consume less energy and resources than conventional semiconductor processes [44]. The design for recycling is simplified as well. A direct comparison between paper and PET substrates for the production of electronic devices showed clear advantages of paper. In almost all of the 18 categories examined in the LCA (e.g. global warming, water use or eutrophication, stratospheric ozone depletion, or ecotoxicity) the use of a paper substrate would cause only 10-20% of the impact of PET. Manuscripts of these results has been submitted to ACS Sustainable Chemistry & Engineering (Glogic et al, 2021).

Although this paper has taken sustainable approach in some aspects there are still development needs towards more environmentally friendly solutions. Main sources of climate impacts and sustainability challenges in the printed electronics typically stem from the fossil-based substrate materials and metals used [45, 46].

Besides paper substrates, there are also other sustainable substrate candidates, including compostable and biodegradable biopolymers as well as other cellulose-based materials. Biodegradation in electronics is a specific area focused on applications such as biomedical applications placed inside the body, drug delivery or therapeutics, as well as environmental sensing and monitoring applications. Biodegradation of materials and components is important also in applications, which most probably enter up in nature in the end of their life time. The research efforts and applications in these areas are increasing and enabled by e.g. novel biodegradable substrate materials. [47–49]

Many of the printed devices utilize silver based inks as the conductive material, also our anti-counterfeit label. Silver has high environmental impact due to its mining process as a side-product from other mines, among other reasons. Its high cost is also an economic issue. Replacement of silver with other metals, such as copper or aluminium, could lower the environmental impact, but even better option would be to use carbon based materials, or replace part of the metals with carbon [50]. Another sustainability issue for metal inks is sintering at high temperature, since many biopolymer and paper based substrates are heat sensitive materials. Therefore, carbon-based materials, such as carbon paste, carbon nanotubes or graphene, have been considered as alternative to metals at least in low conductivity applications [12]. Ink sustainability can also be increased by formulating the ink vehicle from renewable materials, and by using low or no volatile organic compounds.

Another challenge is how to separate electronic material fractions, such as metals, for recycling and reuse [51]. As e.g. the anti-counterfeit label studied in this paper would be small in size, it would most likely end up in the shredder light fraction, which typically goes to energy utilization. In the future with higher price level and more sophisticated technologies, there is, however, potential for separation of some metals or other substances. Recycling of product components can be further advanced through circular product design, including easy removability before paper repulping processes.

As it can be seen on the Table 2, in our experiments the major cost contribution of the smart label is the NFC chip, which represents almost two third of the final cost whereas electricity and man power at VTT is the second cost contributor with almost one quarter of the price. However, man power costs will be lower in an industrial printing unit, since the printing experiments for this paper were carried out at VTT's experimental pilot scale facilities. The printing itself has less impact on the cost of the device (9.47 % of the total cost, i.e. 0.177 €/device) and should also decrease if printed in high volume.

A good way to decrease the price of the ECD fabrication consists in searching for other chips with less functionalities than the one currently used (AMSAS39513). Using a printed rectifier instead of a chip pick-and-place might be also a good way to decrease the cost in order to make ECD more accessible for a daily use.

5 Conclusions

This paper has demonstrated manufacturing of an electronic anti-counterfeit label based on an ECD element and an NFC tag on a paper substrate. This label has been fully processed in R2R pilot-scale consisting of 11 printed layers and an assembled NFC chip. The ECD element was functional and the tags were detectable with a mobile phone integrated NFC reader.

Table 2 Cost estimation for R2R printing and chips pick-and-place for the smart label

Cost item	Price	Printed volume per device (cm^3)	Price per device	Price contribution
Paper (HD-95)	1.2 €/m^3		0.0088 €	0.47%
Silver ink	1640 €/kg	19 cm^3	0.04 €	2.14%
Carbon ink	570 €/kg	8.8 cm^2	0.002 €	0.11%
Dielectric ink	930 €/kg	3x9.1 + 7.1 cm^2	0.06 €	3.21%
Electrochromic ink	980 €/kg	1.8 cm^2	0.0002 €	0.01%
Electrolyte	920 €/kg	2 x 5.7 cm^2	0.046 €	2.46%
Printing plates 1.07%	150	€/piece	11 plates	0.02 €
Chip (AMS AS39513) 63.74%	1.19	€/piece	1	1.19 €
Electricity & man power (incl. machine cleaning)			0.50 €	26.78%
Total			**~1.8 €**	**100%**

All the layers can be successfully printed at good quality and with well-defined edges onto the paper substrate as well as on the top of each other using the R2R rotary screen printing process. In total, over 2000 printed devices without chip were manufactured which corresponds to the total run length of 80 m. With the R2R chips pick-and-place, a very satisfying fabrication yield was obtained (96.5%), however the process still needs some optimization in terms of UV/temperature curing to obtain the highest electrochemical and optical performances. Good ECD performance were obtained with an optical contrast higher than 15 for ECD, and a switching time lower than 5s for a fully printed plastic-free and ITO-free display.

Use of paper as a substrate material is the first step towards more environmentally friendly electronic solutions. In the future, also more sustainable ink options than silver particle inks could be considered. Another option is to include more eco-design aspects in order to minimize the use of harmful metals and to enable more efficient recycling and reuse concepts.

Acknowledgements Research leading to this paper was carried out in Supersmart research project [52] that has received funding from the European Institute of Innovation and Technology (EIT), a body of the European Union, under the Horizon 2020, the EU Framework Programme for Research and Innovation. The project demonstrators were awarded the 'Best Publicly Funded Project Demonstrator' at OE-A Competition 2021.

Part of the facilities used were provided by the Academy of Finland Research Infrastructure "Printed Intelligence Infrastructure (PII-FIRI, grant no. 32020).

The authors would like to thanks the company Gulplug (https://www.gulplug.fr/save-it-yourself/) for gratefully providing the equipments needed for the measurement of the process electrical consumption.

Funding Open access funding provided by Technical Research Centre of Finland (VTT). Research leading to this paper was carried out in Supersmart research project [52] that has received funding from the European Institute of Innovation and Technology (EIT), a body of the European Union, under the Horizon 2020, the EU Framework Programme for Research and Innovation.

Data availability All data generated or analysed during this study are included in this published article.

Code availability Not applicable

Declarations

Ethics approval The authors declare no ethics issues.

Consent to participate & for publication The work described here has not been published before (except as part of a published lecture). The work is not under consideration for publication elsewhere. Its publication has been approved by all co-authors. Its publication has been approved by the responsible authorities at the institution where the work is carried out.

Conflict of interest The authors declare no competing interests.

References

1. United States Environmental Protection Agency. Learn About Sustainability. Available at https://www.epa.gov/sustainability/learn-about-sustainability#what. Accessed 9 Feb 2021

2. European Commission (2018) Sustainable Development Goals: first meeting of the Commission's high level multi-stakeholder platform, Available at: https://ec.europa.eu/commission/presscorner/detail/en/ip_18_82. Accessed 9 Feb 2021
3. EllenMacArthur Foundation, What is the circular economy, Available at https://www.ellenmacarthurfoundation.org/circular-economy/what-is-the-circular-economy. Accessed 9 Feb 2021
4. Kuehr R (2020). E-waste–the underestimated challenge. E-Waste World Conference & Expo, 18-19 Nov. 2020.
5. Forti V, Baldé CP, Kuehr R, Bel G. The Global E-waste Monitor 2020. UNU/UNITAR and ITU, 2020. ISBN Digital: 978-92-808-9114-0. Available online: http://ewastemonitor.info/wp-content/uploads/2020/12/GEM_2020_def_dec_2020-1.pdf. Accessed 11 Feb 2021
6. Ellen MacArthur Foundation (2017) Circular consumer electronics: an initial exploration
7. Payet R (2020). E-waste continues to dominate the environmental agenda on waste management. Available at: http://www.brsmeas.org/?tabid=4332&blogId=5190. Accessed 10 Feb 2021
8. European Union reflection paper (2019) Towards a Sustainable Europe by 2030
9. Hakola L (2020) Five ways towards sustainable electronics. VTT blog post. Available at: https://www.vttresearch.com/en/news-and-ideas/five-ways-towards-sustainable-electronics. Accessed 10 Feb 2021
10. Hakola L, Immonen K, Sokka L, Välimäki M, Smolander M, Mäntysalo M et al (2020) Sustainable materials and processes for electronics, photonics and diagnostics. Proceedings of Electronics Goes Green 2020+, Berlin, pp 45–52
11. Hakola L, Smolander M (2019) Sensing solutions for intelligent packaging supporting circular economy and IoT. Open Dent J 20: 18–19
12. Välimäki MK, Sokka LI, Peltola HB, Ihme SS, Rokkonen TM, Kurkela TJ, Ollila JT, Korhonen AT, Hast JT (2020) Printed and hybrid integrated electronics using bio-based and recycled materials—increasing sustainability with greener materials and technologies. Int J Adv Manuf Technol 111(1):325–339
13. Rifkin ,J(2014) Beyond Obama's Plan: A New Economic Vision for Addressing Climate Change, Huffington Post, available at: www.huffingtonpost.com. Accessed 11 Feb 2021
14. Kanth RK, Wan Q, Lijeberg P, Tuominen A, Zheng L-R, Tenhunen, H (2010) Investigation and Evaluation of Life Cycle Assessment of Printed Electronics and its Environmental Impacts Analysis, Proceedings of NEXT 2010 Conference
15. Müller H, Colley A, Häkkilä J, Jensen W, Löchtefeld M (2019) Using electrochromic displays to display ambient information and notifications. UbiComp/ISWC '19 Adjunct: Adjunct Proceedings of the 2019 ACM International Joint Conference on Pervasive and Ubiquitous Computing and Proceedings of the 2019 ACM International Symposium on Wearable Computers pp. 1075–1078
16. Andersson Ersman P, Zabihipour M, Tu D, Lassnig R, Strandberg J, Åhlin J, Nilsson M, Westerberg D, Gustafsson G, Berggren M (2020) Monolithic integration of display driver circuits and displays manufactured by screen printing. Flexible Printed Electron 5, (2)
17. Andersson Ersman P, Lassnig R, Strandberg J, Dyreklev P (2021) Flexible Active Matrix Addressed Displays Manufactured by Screen Printing. Adv Eng Mater 23:2000771
18. Lee J, Lee Y, Ahn J (2017) Improved electrochromic device performance from silver grid on flexible transparent conducting electrode prepared by electrohydrodynamic jet printing. J Mater Chem C 48
19. Pietsch M, Rödlmeier T, Schlisske S, Zimmermann J, Romero-Nieto C, Hernandez-Sosa G (2019) Inkjet-printed polymer-based electrochromic and electrofluorochromic dual-mode displays. J Mater Chem C 7:7121–7127
20. Levasseur D, Mjejri I, Rolland T, Rougier A (2019) Colour tuning by oxide addition in PEDOT:PSS-based electrochromic devices. Polymers 11(1):179
21. Wei Y, Wang X, Torah R, Tudor J (2017) Dispenser printing of electrochromic display on textiles for creative applications. Electron Lett 53(12):779–781
22. Pietsch M, Schlisske S, Held M, Strobel N, Wieczorek A, Hernandez-Sosa G (2020) Biodegradable inkjet-printed electrochromic display for sustainable short-lifecycle electronics. J Mater Chem C 8:16716–16724
23. Brooke R, Mitraka E, Sardar S, Sandberg M, Sawatdee A, Berggren M, Crispin X, Jonsson MP (2017) Infrared electrochromic conducting polymer devices. J Mater Chem C 5:5824–5830. https://doi.org/10.1039/C7TC00257B
24. Barras R, Cunha I, Gaspar D, Fortunato E, Martins R, Pereira L (2017) Printable cellulose-based electroconductive composites for sensing elements in paper electronics. Flex Printed Electron 2(1):12
25. Sappati KK, Bhadra S (2018) Piezoelectric Polymer and Paper Substrates: A Review. Sensors 18(11):3605–3630
26. Gaspar C, Olkkonen J, Passoja S, Smolander M (2017) Paper as Active Layer in Inkjet-Printed Capacitive Humidity Sensors. Sensors 17(7):10
27. Danine A, Manceriu L, Faure C, Labrugère C, Penin N, Delattre A, Eymin-Petot-Tourtollet G, Rougier A (2019) Toward Simplified Electrochromic Devices Using Silver as Counter Electrode Material. ACS Appl Mater Interfaces 11(37):34030–34038
28. Vishtal A, Retulainen E (2012) Deep-drawing of paper and paperboard: The role of material properties. BioResources 7(3):4424–4450
29. Sullivan M. (2018) Printed Electronics: Global Markets to 2022, BCC Research LLC.
30. Sohail M, Sun D-W, Zhu Z (2018) Recent developments in intelligent packaging for enhancing food quality and safety. Crit Rev Food Sci Nutr 58(15):2650–2662
31. Wang Y, Yan C, Cheng S-I, Xu Z-Q, Sun X, Xu Y-H, Chen J-J, Jiang Z, Liang K, Feng Z-S (2019) Flexible RFID Tag Metal Antenna on Paper-Based Substrate by Inkjet Printing Technology. Adv Funct Mater 2019(29):1902579
32. Islam MT, Alam T, Yahya I, Cho M (2018) Flexible Radio-Frequency Identification (RFID) Tag Antenna for Sensor Applications. Sensors 2018(18):4212
33. Nunes D, Freire T, Barranger A, Vieira J, Matias M, Pereira S, Pimentel A, Cordeiro NJA, Fortunato E, Martins R (2020) TiO2 Nanostructured Films for Electrochromic Paper Based-Devices. Appl Sci 2020(10):1200
34. Lang AW, Österholm AM, Reynolds JR (2019) Paper-Based Electrochromic Devices Enabled by Nanocellulose-Coated Substrates. Adv Funct Mater 2019(29):1903487
35. Andersson Ersman P, Lassnig R, Strandberg J, Tu D, Keshmiri V, Forchheimer R, Fabiano S, Gustafsson G, Berggren M (2019) All-printed large-scale integrated circuits based on organic electrochemical transistors. Nat Commun 10:5053
36. Kirchmeyer S (2016) The OE-A roadmap for organic and printed electronics: creating a guidepost to complex interlinked technologies, applications and markets. Transl Mater Res 3(1)
37. Furuta T, Tonooka H, Kobayashi M (2008) Research on Recycling Cardboard with RF Tags/Labels. RENGO CO., LTD. The Eighth International Conference on EcoBalance, Tokyo
38. Erdmann L, Hilty L, Althaus H-J (2009). Einfluss von RFID-Tags auf die Abfallentsorgung: Prognose möglicher Auswirkungen eines massenhaften Einsatzes von RFIDTags im Konsumgüterbereich auf die Umwelt und die Abfallentsorgung. Dessau-Roßlau: Umweltbundesamt.
39. Aliaga C, Zhang H, Dobon A, Hortal M, Beneventi D (2015) The influence of printed electronics on the recyclability of paper: a case

study for smart envelopes in courier and postal services. Waste Manag 38:41–48
40. Schacfcr D, Chcung WM (2018) Smart Packaging: Opportunities and Challenges. Procedia CIRP 72:1022–1027
41. Chen S, Yi J, Zhu X, Jiang H, Ju W (2017) RFID-based integrated method for electromechanical products disassembly decision-making. International Journal of Computer Integrated Manufacturing, 30(2–3)
42. 'Colourimetry — (2021) Part 4: CIE 1976 L*a*b* colour space | CIE'. http://cie.co.at/publications/colourimetry-part-4-cie-1976-lab-colour-space-1 (accessed March. 12,)
43. Choudhury AKR (2010) 2 - Scales for communicating colours, in Colour Measurement, M. L. Gulrajani, Ed. Woodhead Publishing, 2010, pp. 19-e3
44. Zheng R, Tenhunen H, Zou Z (2018) Life Cycle Assessment (LCA) for Printed Electronics, in Smart Electronic Systems, John Wiley & Sons, Ltd, pp. 243–267
45. Liu J, Yang C, Wu H, Lin Z, Zhang Z, Wang R, Wong CP (2014) Future paper based printed circuit boards for green electronics: fabrication and life cycle assessment. Energy Environ Sci 7(11):3674–3682
46. Espinosa N, García-Valverde R, Urbina A, Lenzmann F, Manceau M, Angmo D, Krebs FC (2012) Life cycle assessment of ITO-free flexible polymer solar cells prepared by roll-to-roll coating and printing. Sol Energy Mater Sol Cells 97:3–13
47. Feig VR, Tran H, Bao Z (2018) Biodegradable Polymeric Materials in Degradable Electronic Devices. ASC Cent Sci 4:337–348
48. Li L, Wang D, Kong YL (2018) Recent progress on biodegradable materials and transient electronics. Bioactive Mater 3:322–333
49. Feig VR, Tran H, Bao Z (2018) Biodegradable Polymeric Materials in Degradable Electronic Devi. ACS Central Sci 4(3):337–348
50. Slotte M, Zevenhoven R (2017) Energy requirements and life cycle assessment of production and product integration of silver, copper and zinc nanoparticles. J Clean Prod 148:948–957
51. Widmer R, Oswald-Krapf H, Sinha-Khetriwal D, Schnellmann M, Böni H (2005) Global perspectives on e-waste. Environ Impact Assess Rev 25(5):436–458
52. Supersmart project webpages, available at https://supersmart-project.eu/. Accessed 21 Feb 2021